# Unidirectional Propagation of Chemical Waves through Microgaps between Zones with Different Excitability

**Kenji Suzuki,* Tatsuo Yoshinobu, and Hiroshi Iwasaki**

*The Institute of Scientific and Industrial Research, Osaka University, 8−1 Mihogaoka, Ibaraki, Osaka 567-0047, Japan*

*Received: February 22, 2000; In Final Form: May 1, 2000*

Unidirectional propagation of chemical waves in the Belousov−Zhabotinsky (BZ) reaction system was demonstrated using patterns of a BZ catalyst on a cation-exchange membrane. The unidirectional propagation was observed when the chemical waves entered catalyst-less microgaps separating catalyst zones with different thicknesses on the membrane. The chemical waves could pass through the microgaps from a thinner catalyst zone and could not pass through the microgaps from a thicker catalyst zone. The study shows that the asymmetry of excitability of the both zones and the gap width between them are key factors that caused the unidirectional propagation. Computer simulations reproduce the unidirectional propagation.

## Introduction

Chemical waves propagating in Belousov−Zhabotinsky (BZ) solutions have been thought to be a convenient model of waves in biological excitable media such as heart muscles and brain tissues.[1−3] Most of the basic properties of the chemical waves have been revealed by experimental and theoretical studies on the chemical waves observed in spatially uniform BZ solutions.[4−6] Recently, the propagation of chemical waves in inhomogeneous BZ systems has also come to occupy an important position in studies on the chemical waves,[7−19] because biological excitable media are clearly inhomogeneous. The effects of geometrical shapes[9−14] and inhomogeneity of refractoriness[15,16] or excitability[17,18] of the excitable BZ media on the chemical wave propagation can be investigated by using modified BZ systems with fixed catalysts.

Most recently, Agladze et al. have demonstrated a "chemical diode" that realizes the unidirectional propagation of chemical waves in excitable BZ media by its asymmetric geometry.[19] The unidirectional propagation of chemical waves is one of the most interesting phenomena observed in nonuniform BZ reaction media, because it is closely connected with signal processing in excitable media.[19−23] In their studies, the unidirectional propagation of the chemical waves highly relies on the two-dimensional shape of the BZ reaction media.

In this study, we investigated the chemical wave propagation on the catalyst pattern on a cation-exchange membrane and found another type of unidirectional propagation of the chemical waves through a catalyst-less microgap separating two catalyst zones with different thicknesses. The experimental results clearly indicate that the unidirectional propagation is due to the asymmetrical excitability of BZ media as a result of the difference in thickness of catalyst zones. The dependence of excitability of BZ media on its thickness can be explained in terms of the dissipation of the activator from the membrane surface. Numerical simulations in a one-dimensional system are performed to confirm the experimental results, assuming dissipation of the activator.

This type of unidirectional propagation should have a close connection with pattern formation of waves in excitable media with inhomogeneous excitability, since asymmetry of excitability may exist widely in real excitable systems with spatially inhomogeneous excitability.

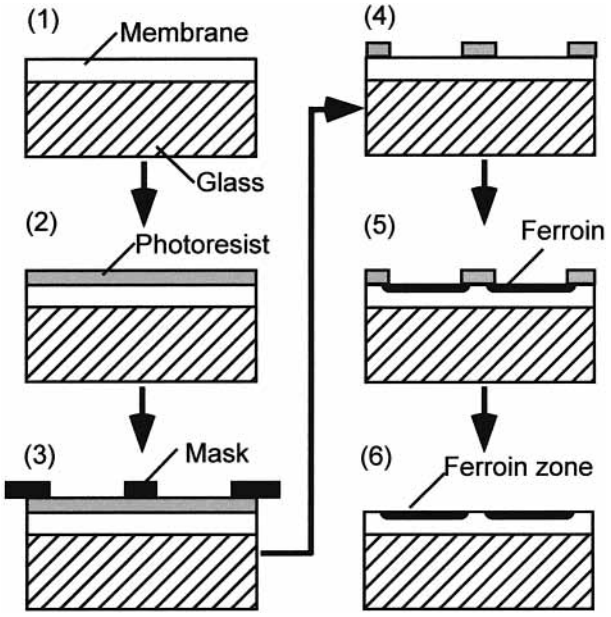


**Figure 1.** Process sequence of catalyst patterning on a cation-exchange membrane.

## Experimental Section

**Photolithographic Process.** Figure 1 shows the photolithographic process employed in this study.[24] A cation-exchange membrane of 0.18 mm in thickness (DUPONT Nafion 117 perfluorosulfonic acid membrane) was immersed in hot water at 90 °C for 1 h and was fixed on a glass plate by silicone rubber (Shin-Etsu Chemical Co., Ltd., 1Component RTV KE45). A positive G-line photoresist (Shipley Far East S1818) was spin-coated onto the membrane. The membrane was covered with a mask, on which the desired pattern is printed during exposure to the light from a mercury lamp. Then, the membrane was immersed in a developer (Shipley Far East MF-CD26) and rinsed in deionized water. Thereafter, it was immersed in an

* Corresponding author. E-mail: kenji31@sanken.osaka-u.ac.jp.

10.1021/jp0007078 CCC: $19.00 © 2000 American Chemical Society
Published on Web 06/21/2000

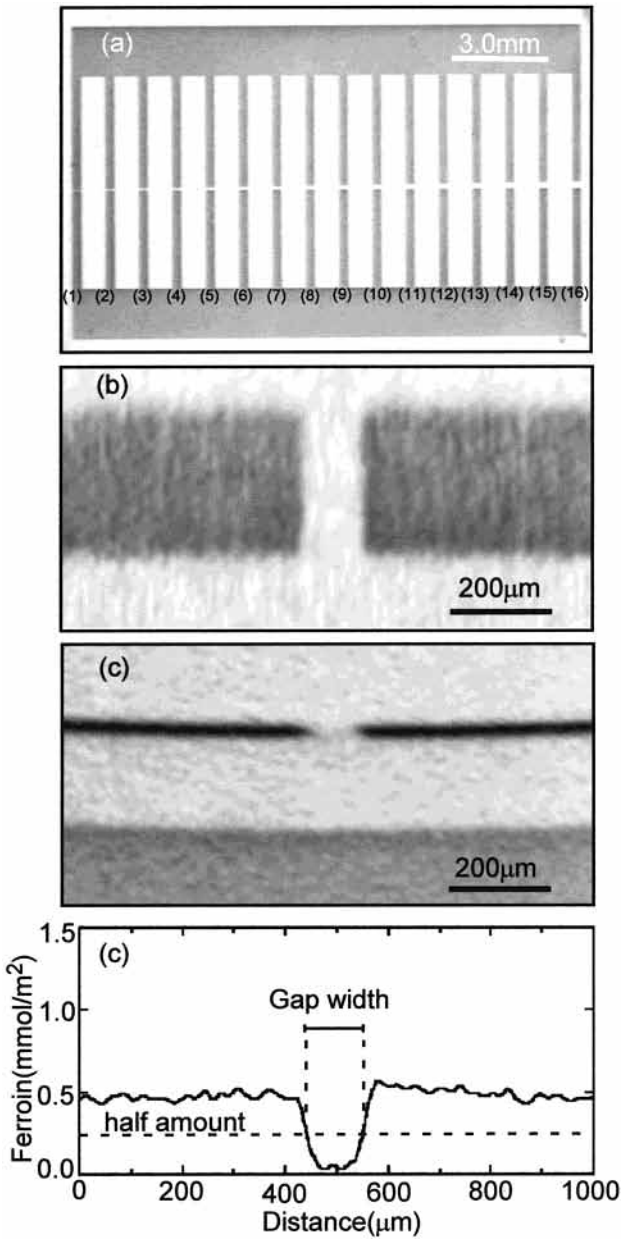


**Figure 2.** Ferroin pattern with 16 symmetric microgaps on the cation-exchange membrane (Nafion 117): (a) photograph of the whole catalyst pattern; (b) enlarged photograph of the symmetric microgap on vertical line no. 9; (c) photograph of the cross section of the membrane around the symmetric microgap on vertical line no. 9; (d) spatial distribution of the ferroin concentration around the symmetric microgap on vertical line no. 9.

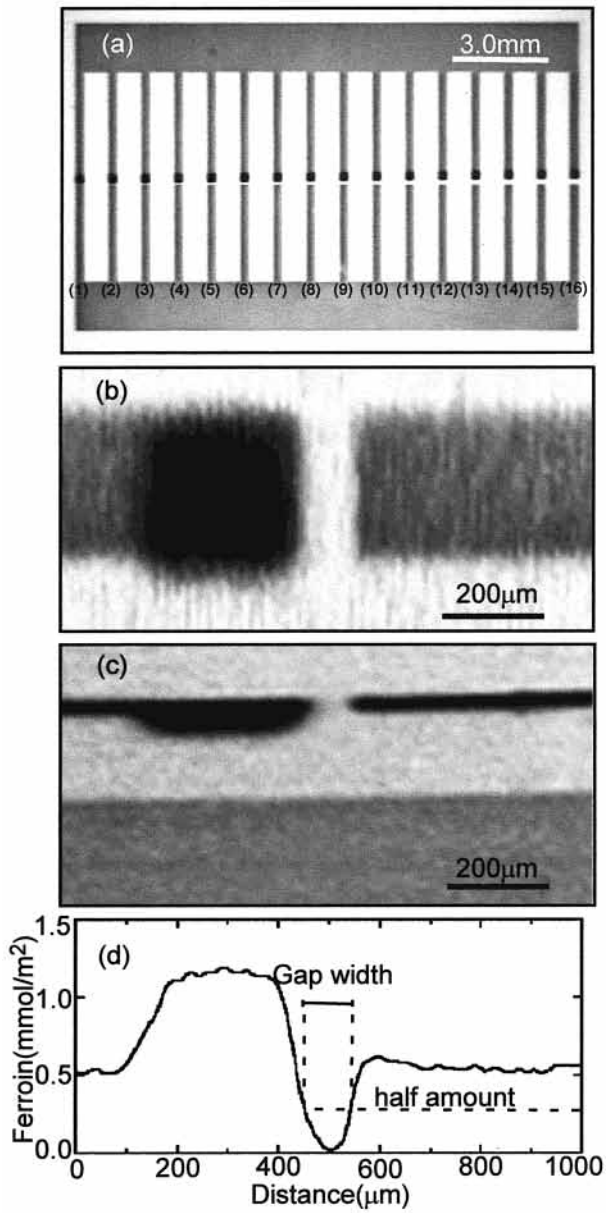


**Figure 3.** Ferroin pattern with 16 asymmetric microgaps on the cation-exchange membrane (Nafion 117): (a) photograph of the whole catalyst pattern; (b) enlarged photograph of the asymmetric microgap on vertical line no. 9; (c) photograph of the cross section of the membrane around the asymmetric microgap on vertical line no. 9; (d) spatial distribution of the ferroin concentration around the asymmetric microgap on vertical line no. 9.

aqueous solution of ferroin for 30 s to immobilize ferroin, which functions as a catalyst in the BZ reaction. The ferroin molecules $[Fe(phen)_3]^{2+}$ are bonded to sulfonate groups ($-SO^{3-}$) in the membrane. The photoresist on the membrane was removed by ethanol. The membrane was immersed in deionized water for 24 h in order to remove the ethanol and other contaminants.

**Fabrication and Characterization of Catalyst Micro Patterns.** By the photolithographic method, two types of catalyst (ferroin) patterns on the membranes were made. One is a pattern with symmetric microgaps. The other is a pattern with asymmetric microgaps.

The former consists of two horizontal lines connected by 16 vertical lines, as shown in Figure 2a. Each of the vertical lines has the symmetric microgap near its center. Since the widths of the gaps on the mask for the photolithographic process, corresponding to the symmetric microgaps on vertical lines 1−16, were 50−200 $\mu$m, respectively, the width of the symmetric microgap increases from left to right, as shown in Figure 2a. This pattern can be fabricated by carrying out the photolithographic process only once. The composition of the aqueous solution of ferroin used in the photolithographic process was as follows: [ferroin] = 2.5 mM, [ethanol] = 16 M. Figure 2b shows a top view of the symmetric microgap on vertical line no. 9 in Figure 2a. Black regions correspond to the zones loaded with ferroin. Figure 2c shows the cross section of the membrane along the center of vertical line no. 9. A membrane was cut with a razor in order to observe the cross section. The cross sections of the membrane were observed with an optical microscope. The thickness of the membrane becomes 200 $\mu$m, since the membrane has swollen in water. The thickness of the catalyst zone loaded with ferroin is about 30 $\mu$m. Figure 2d

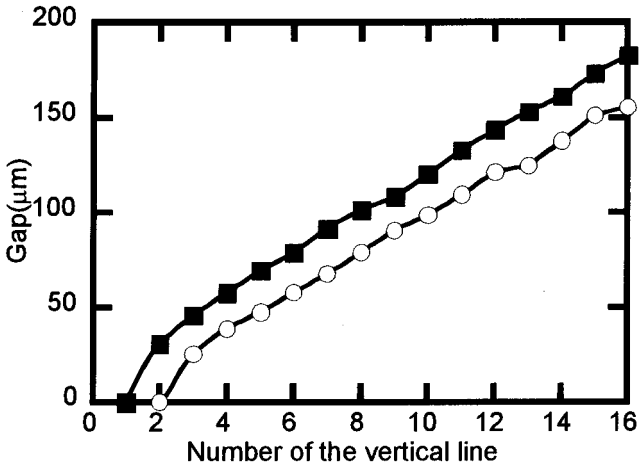


**Figure 4.** Gap widths of both the symmetric microgaps (■) and the asymmetric microgaps (○).

shows the spatial distribution of the amount of ferroin around the symmetric microgap along the center of vertical line no. 9. The amount of ferroin was calculated by comparing the brightness of the pattern in the CCD image with that of the standard membranes, for which the amount of ferroin was previously determined by a UV−vis spectrometer. The amounts of ferroin at both sides of the symmetric microgap are almost the same (0.5 mmol/m$^2$). The average concentration of ferroin in the ferroin zone is estimated at 17 mM. Spreading of the ferroin molecules near the edge of the microgap is observed. This is mainly due to the process of photoresist removal by ethanol. The gap width of the symmetric microgap was defined as the distance between two points where the amount of ferroin becomes half of the amount in the vertical line. The gap width is shown in Figure 4. The gap width of the symmetric microgap on vertical line no. 1 is zero because of the spreading of the ferroin pattern.

The pattern with asymmetric microgaps differs from the former in that each asymmetric microgap has a zone loaded with a large amount of ferroin (a catalyst zone L) immediately above the microgap, as shown in Figure 3a. The lower side of the microgap corresponds to a zone loaded with a relatively small amount of ferroin (a catalyst zone S). This pattern was fabricated by repeating the photolithographic process twice. At first, a catalyst pattern consisting of 16 square patterns corresponding to the catalyst zones L above the gaps was fabricated on a cation-exchange membrane. The composition of the aqueous solution of ferroin used in the photolithographic process was as follows: [ferroin] = 12.5 mM, [ethanol] = 16 M. Next, the same pattern as the symmetric microgap was fabricated on the cation-exchange membrane in the proper position. The composition of the aqueous solution of ferroin used was the same as that used for the fabrication of the symmetric microgap. Figure 3b shows the top view of the asymmetric microgap on vertical line no. 9 in Figure 3a. Figure 3c shows the cross section of the membrane along the center of vertical line no. 9. The depth of the catalyst zone L is about 65 $\mu$m, and the depth of the catalyst zone S is about 30 $\mu$m. Figure 3d shows the spatial distribution of the amount of ferroin along the center of vertical line no. 9. The average ferroin concentrations in the catalyst zones L and S are about 18 and 17 mM, respectively. The gap width of the asymmetric microgap was defined as the distance between two points where the amount of ferroin becomes half of that on catalyst zone S. The gap width is shown in Figure 4. The gap widths of the symmetric microgaps on vertical lines 1 and 2 are zero because of the spreading of the ferroin pattern.

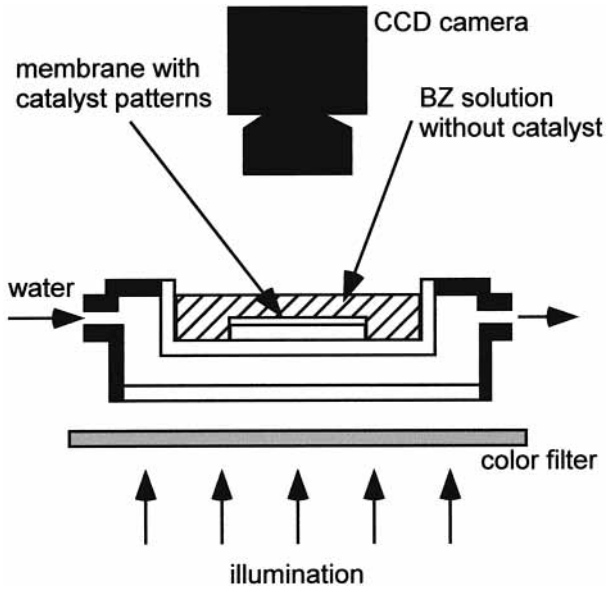


**Figure 5.** Schematic illustration of the side view of the experimental setup.

To sum up, since the average ferroin concentrations of the catalyst zone L and the catalyst zone S are almost the same, the difference between the catalyst zone L and the catalyst zone S is only the thickness of the zones. Accordingly, the symmetric microgap consists of two of the thin catalyst zones S, while the asymmetric microgap consists of the thick catalyst zone L and the thin catalyst zone S.

**Pretreatment of the Catalyst Patterns on the Membrane.** Prior to all experiments, the membranes with catalyst patterns were immersed in an aqueous solution ([$H_2SO_4$] = 1.5 M, [$NaBrO_3$] = 1 M) for 3 h in order to decompose the ethanol left in the membrane by the oxidation reaction with the bromate. During the latter half of the immersion process, the color of the catalyst pattern turned from red to blue. This is the sign of the end of the oxidation process. The membrane was rinsed in deionized water and stored in an aqueous solution ([$H_2SO_4$] = 0.1 M). The color of the catalyst patterns gradually returned from blue to red.

**Experimental Setup.** Figure 5 shows the configuration of our experiment. The patterned membrane on a glass plate was immersed in the BZ solution without catalyst. The initial compositions of the BZ solution were as follows: [$H_2SO_4$] = 0.50−1.0 M, [$NaBrO_3$] = 0.4 M, [$CH_2(COOH)_2$] = 0.4 M, [NaBr] = 0.08 M. The depth of the solution was about 10 mm, and the temperature of the solution was maintained at 25.0 ± 0.5 °C by a constant flow of 24.5 °C water through the heat bath. In this solution, the catalyst patterns on a membrane worked as excitable media and the chemical wave never appeared spontaneously. The catalyst pattern is red in the solution and the front of the chemical waves is blue. Both the upper and the lower walls of the heat bath are made of transparent glass plates, so that the membrane can be illuminated by the light of a halogen lamp from the bottom through a blue filter (50%T at 441 nm). The changes between red and blue were recorded as the change in the light intensity by a black-and-white CCD camera (Sony XC-77) connected to a video cassette recorder.

## Results and Discussion

**Results of Experiments.** Figure 6 shows the dependence of the propagation probability of the chemical waves through the

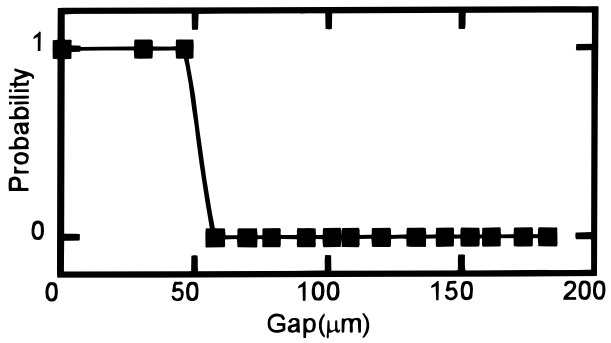


**Figure 6.** Dependence of propagation probability of the chemical waves through the symmetric microgap on the gap width ($[H_2SO_4] = 0.50$ M, $[NaBrO_3] = 0.4$ M, $[CH_2(COOH)_2] = 0.4$ M, $[NaBr] = 0.08$ M).

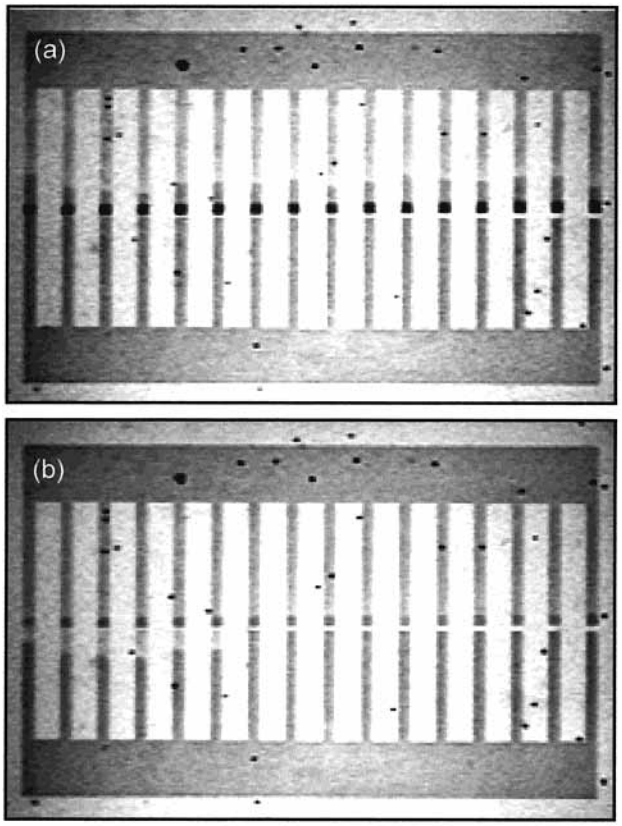


**Figure 7.** Successive photographs of the L → S propagation of the chemical waves through the asymmetric microgaps at an interval of 120 s ($[H_2SO_4] = 0.50$ M, $[NaBrO_3] = 0.4$ M, $[CH_2(COOH)_2] = 0.4$ M, $[NaBr] = 0.08$ M).

symmetric microgap on the gap width. The critical gap width $g_c$(S → S) (i.e., the gap width above which no chemical waves propagate though the gap from one catalyst zone (S) to the other catalyst zone (S)) of the S → S propagation is estimated at 50 $\mu$m. Naturally, this symmetric microgap never shows the unidirectional propagation of the chemical waves.

Figure 7 shows the photographs of the L → S propagation (i.e., the propagation of the chemical waves from the thick catalyst zone L to the thin catalyst zone S) of the chemical waves through the asymmetric microgaps. For each of the microgaps in Figure 7a, a single chemical wave is going down on the vertical line above the microgap. And then the chemical waves only on microgaps on vertical lines 1−6 can propagate through the asymmetric microgaps, as shown in Figure 7b. The $g_c$(L → S) of the chemical wave propagation is estimated to be 60 $\mu$m.

On the other hand, Figure 8 shows the photographs of the S → L propagation of the chemical waves through the asymmetric microgaps. For each of the microgaps in Figure 8a, a single chemical wave is going up on the vertical line below the microgap. And then the chemical waves only on microgaps 1−12 can propagate through the asymmetric microgaps as shown in Figure 8b. The $g_c$(S → L) of the chemical wave propagation is estimated to be 120 $\mu$m.

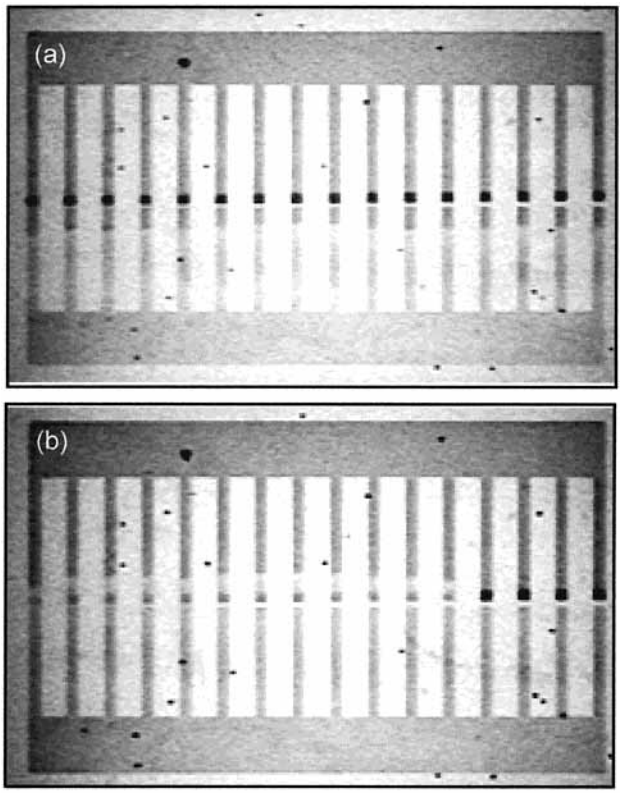


**Figure 8.** Successive photographs of the S → L propagation of the chemical waves through the asymmetric microgaps at an interval of 120 s ($[H_2SO_4] = 0.50$ M, $[NaBrO_3] = 0.4$ M, $[CH_2(COOH)_2] = 0.4$ M, $[NaBr] = 0.08$ M).

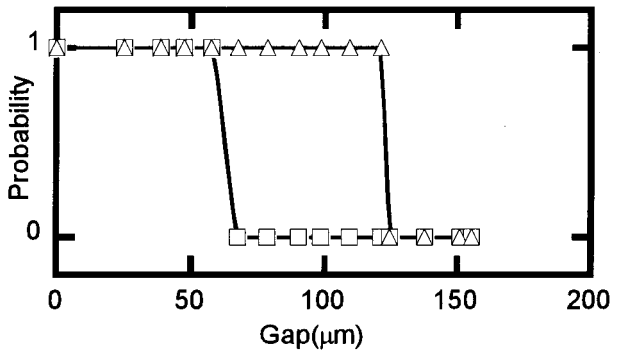


**Figure 9.** Dependence of the propagation probabilities of the chemical waves propagating through the asymmetric microgap in both the L → S direction (□) and S → L direction (△) on the gap width ($[H_2SO_4] = 0.50$ M, $[NaBrO_3] = 0.4$ M, $[CH_2(COOH)_2] = 0.4$ M, $[NaBr] = 0.08$ M).

Figure 9 summarizes the dependence of the propagation probabilities of the chemical waves propagating through the asymmetric microgap in both L → S and S → L directions on the gap width. For gap widths from 60 to 120 $\mu$m, chemical waves can pass through the asymmetric microgap in the S → L direction, but cannot in the opposite direction. Therefore, for these gap widths, the asymmetric microgap works as a kind of "chemical diode" and the S → L direction corresponds to the forward direction.

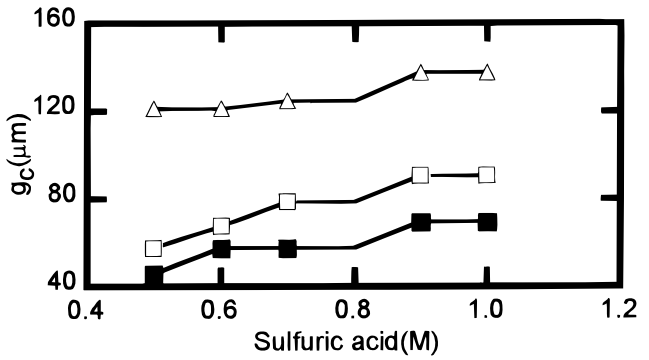


**Figure 10.** Dependence of the values of $g_c(S \rightarrow S)$ (■), $g_c(L \rightarrow S)$ (□), and $g_c(S \rightarrow L)$ (△) on the concentration of sulfuric acid in the BZ solution. For the concentration of sulfuric acid less than 0.5 M, the catalyst zone S loses its excitability. For the concentration of sulfuric acid larger than 1.0 M, the spontaneous generation of the chemical waves disturbs the measurement of the critical gap width.

Figure 10 shows the dependence of the values of the $g_c(S \rightarrow S)$, $g_c(L \rightarrow S)$, and $g_c(S \rightarrow L)$ on the concentration of sulfuric acid in the BZ solution. They tend to increase at almost the same rate as the concentration of sulfuric acid increases. Accordingly, the forward direction of the asymmetric microgap is the same even in a broad range of acidity.

The propagation of chemical waves through catalyst-less gaps has already been reported in earlier papers.[10−14,19−23] The chemical wave propagation can be explained by considering the diffusive transport of activator species $HBrO_2$ though the catalyst-less gaps. The $g_c$ is expected to depend on the amount of the activator species released from the transmitter side of the gap (i.e., one side of a microgap from which chemical waves propagate through the microgap) and the excitability of the BZ reaction media of the receiver side of the gap (i.e., the other side of the microgap to which the chemical waves propagate through the microgap). Here we discuss the mechanism of the unidirectional propagation of the chemical waves based on the relationship between the experimental values of $g_c(S \rightarrow S)$, $g_c(L \rightarrow S)$, and $g_c(S \rightarrow L)$.

When the $L \rightarrow S$ propagation is compared to the $S \rightarrow S$ propagation, $g_c(L \rightarrow S)$ is larger than $g_c(S \rightarrow S)$ by 10 $\mu$m. This is due to the difference of the thickness of the catalyst zone of the transmitter sides in symmetric and asymmetric microgaps, because the catalyst zones of the receiver side of the both microgaps are almost the same. Since the thick catalyst zone L tends to release more activator species than the thin catalyst zone S, the experimental results can be explained in terms of the difference between the amounts of the activator released from the transmitter sides.

On the other hand, when the $S \rightarrow L$ propagation is compared to the $S \rightarrow S$ propagation, $g_c(S \rightarrow L)$ is larger than $g_c(S \rightarrow S)$ by 70 $\mu$m. This is due to the difference of the thickness of the catalyst zone of the receiver sides in symmetric and asymmetric microgaps, because the catalyst zones of the transmitter sides of both microgaps are almost the same. The experimental results suggest that the thick catalyst zone L tends to have a higher excitability than the thin catalyst zone S.

Aliev et al. have reported the phenomenon probably connected with this tendency of excitability, using a similar BZ system of silica gel layer with a fixed-catalyst with gradually decreasing thickness.[25] It has been shown that there is a critical layer thickness below which chemical waves cannot propagate in the gel layers. In their system, the critical layer thickness is about 130 $\mu$m at 20 °C. In addition, Yoshikawa et al. have reported that the frequency of BZ oscillation in small beads decreases with the size of the beads.[26] The dependence of the frequency on bead size was observed for bead sizes from 100 to 400 $\mu$m at 23 °C. Both phenomena have been explained by assuming the dissipation of the activator through the surface of the catalyst supports and are thought to be characteristic of phenomena in BZ media with submillimeter sizes.

To explain our experimental results, we assume a similar dissipation of the activator from the catalyst zones, which is from 30 to 65 $\mu$m in thickness. In our system, the excitation at the receiver side is caused by the activator coming from the transmitter side if the concentration of the activator in the catalyst zone of the receiver side exceeds the threshold value that is decided by the local mass balance of the activator there. Since a decrease in the thickness of the receiver catalyst zone enhances the effect of dissipation of the activator through the membrane surface, a decrease in the thickness of the receiver catalyst zone results in a decrease in the excitability of the receiver side.

The chemical diode reported by Agladze et al. takes advantage of the influence of the asymmetry of the shape of BZ media on the diffusive transmission of the activator through microgaps separating the BZ media. On the other hand, the unidirectional propagation observed in our system is due to the asymmetry of the excitability of the BZ media as a result of the difference in thickness of catalyst zones. Consequently, the mechanism of the unidirectional propagation observed here is different from that of the chemical diode reported by Agladze et al.

**Modeling of the Mass Balance of the Activator.** Next we consider the dependence of the excitability on the thickness of the catalyst zones based on the theoretical framework of the Rovinsky−Zhabotinsky (RZ) model.[27−29] The local mass balance of the activator in the catalyst zone is decided by the relationship between the local chemical reactions and local dissipation of the activator. In the RZ model, local chemical reactions of the two-variable system is given by the dimensionless rate equations

$$\frac{dx}{d\tau} = \frac{1}{\epsilon}\left[x(1-x) - \left(2q\alpha\frac{z}{(1-z)} + \beta\right)\frac{x-\mu}{x+\mu}\right] \qquad (1a)$$

$$\frac{dz}{d\tau} = x - \alpha\frac{z}{1-z} \qquad (1b)$$

where

$$[[Fe(phen)_3]^{3+}] = Cz \qquad [HBrO_2] = \frac{k_1 A}{2k_4}x$$

$$\epsilon = \frac{k_1 A}{k_4 C} \qquad \alpha = \frac{k_4 K_8 B}{(k_1 A h_0)^2} \qquad \mu = \frac{2k_4 k_7}{k_1 k_5}$$

$$t = \frac{k_4 C}{(k_1 A)^2 h_0}\tau \qquad \beta = \frac{2k_4 k_{13} B}{(k_1 A h_0)^2}$$

$$C = [[Fe(phen)_3]^{2+}] + [[Fe(phen)_3]^{3+}] \qquad A = [NaBrO_3]$$

$$B = [CHBr(COOH)_2]$$

and $h_0$ is the acidity function, $q$ is the stoichiometric factor, and $k_i$ are the rate constants.

Here variable $x$ and $z$ represent the dimensionless concentrations of $HBrO_2$ and ferroin, respectively. Next we consider the mass balance of activator in the ferroin zone with thickness $d$ per area $S$ in unit time taking the dissipation of the activator through the surface of the membrane into account.[26] On the other hand, the dissipation of ferroin through the membrane

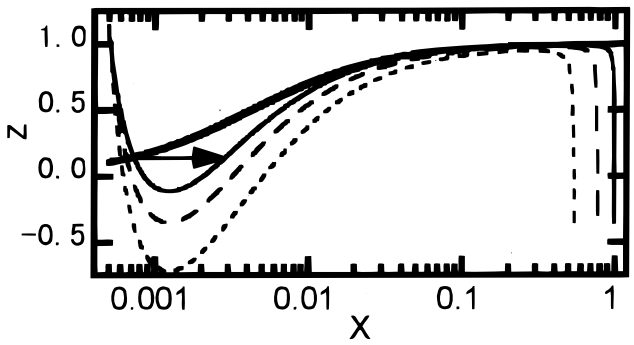


**Figure 11.** *x*-nullcline for eq 2a on *d*. The solid bold line indicates the *z*-nullcline. The solid thin line indicates the x-nullcline for $\eta = 0$. The broken line and dotted line indicate the *x*-nullclines for $d = 60$ and 30 $\mu$m, respectively ($\eta = 30$ $\mu$m, $\epsilon = 4.52 \times 10^{-1}$, $q = 0.5$, $\alpha = 4.25 \times 10^{-3}$, $\beta = 3.4 \times 10^{-3}$, $\mu = 5.1 \times 10^{-4}$, $h_0 = 0.4$).

surface is neglected, since the ferroin molecules are fixed in the membrane. Roughly speaking, the rate of decrease of the concentration of activator by the dissipation of activator through the membrane surface is expected to be proportional to $\eta x/d$, since the rate of the decrease of the amount of the activator in the volume $Sd$ is expected to be proportional to $\eta Sx$. Here $\eta$ is the mass transfer coefficient of the activator through the membrane surface. As a result, the rates of change of the concentrations of activator and ferroin in the catalyst zone are given by

$$\frac{dx}{d\tau} = F(x,z) - \frac{\eta}{d}x \equiv F'(x,z) \tag{2a}$$

$$\frac{dz}{d\tau} = G(x,z) \tag{2b}$$

where $F(x,z)$ and $G(x,z)$ are the right-hand sides of eqs 1a and 1b, respectively. The second term of the right-hand side of eq 2a represents the dissipation of the activator.

Figure 11 shows the dependence of *x*-nullcline for eq 2 on *d*. The points of intersection of the *x*-nullclines and the *z*-nullcline correspond to the steady states for the various values of *d*. Before the arrival of the chemical wave, the system at the catalyst zone of the receiver side is at the corresponding steady state for each value of *d* and is waiting the arrival of the activator released from the transmitter side subsequently to the arrival of a chemical wave at the transmitter side. When the activator released from the transmitter side reaches the receiver side, the system is shifted in the direction of increasing *x*. If the system is shifted to the right of the middle branch of the *x*-nullcline, a new excitation is initiated at the receiver side and a chemical wave propagates through the gap. Obviously, the distance between its steady state and its middle branch can be used as a good measure of the excitability of the catalyst zone. The larger the distance is, the smaller the excitability is. Accordingly, as shown in Figure 11, excitablility of a thick catalyst zone is larger than a thin catalyst zone.

Finally, we show the one-dimensional simulation of the chemical wave propagation through catalyst-less microgaps separating two catalyst zones with different thicknesses. The reaction−diffusion equations at catalyst zones are given by

$$\frac{dx}{d\tau} = F'(x,z) + \Delta_\rho x \tag{3a}$$

$$\frac{dz}{d\tau} = G(x,z) \tag{3b}$$

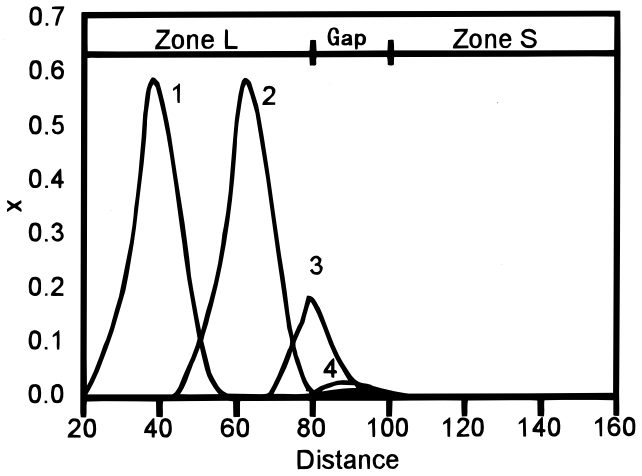


**Figure 12.** Concentration profiles of *x* along the spatial axis (grid points) at equal time intervals for the L → S propagation. The left side and the right side of the gap are the zones with thickness of 60 $\mu$m (zone L) and 30 $\mu$m (zone S), respectively. The chemical wave fails to propagate through the gap ($\eta = 30$ $\mu$m, $\epsilon = 4.52 \times 10^{-1}$, $q = 0.5$, $\alpha = 4.25 \times 10^{-3}$, $\beta = 3.4 \times 10^{-3}$, $\mu = 5.1 \times 10^{-4}$, $\Delta\tau = 5 \times 10^{-3}$, $h_0 = 0.4$).

where $r$ is a spatial coordinate, $\rho$ is the scaled spatial coordinate, and $\Delta_\rho$ is the Laplacian operator with respect to coordinates $\rho$. The scaling of the $\rho$ coordinates is given by the expression[29]

$$\rho = r\left[\frac{k_1^2 A^2 h_0}{k_4 C D_x}\right]^{1/2}$$

We assume that $D_x = 2 \times 10^{-7}$ cm$^2$ s$^{-1}$, which is $^1/_{100}$th of the value of $D_x$ in aqueous BZ solutions, because the velocity of the chemical waves in Nafion membrane is expected to be less than 10% of that in aqueous BZ solution.[30−31]

The reaction−diffusion equation at the microgap is given by

$$\frac{dx}{d\tau} = -\frac{1}{\epsilon}x^2 + \Delta_\rho x \tag{4}$$

where the first term of the right-hand side is the term of the disproportionation reaction of $HBrO_2$.[10]

The computations were carried out in a one-dimensional line of 180 grid points using the explicit Euler method of integration. The microgap was defined as a line of $n$ grid points ($n < 40$) occupying the center of the line of 180 grid points. Following Aliev and Rovinsky,[29] the rate constants rescaled for 20 °C were used.

As shown in Figures 12 and 13, in a certain range of the gap width, the chemical waves simulated based on eqs 3a, 3b, and 4 could pass through the asymmetric microgap only in the S → L direction, although the amplitude of the chemical wave on zone L is larger than that on zone S. This model successfully reproduces the unidirectional propagation of the chemical wave in which the asymmetry of the excitability of BZ media plays a dominant role. Figure 14 shows the dependence of the values of the $g_c$(S → S), $g_c$(L → S), and $g_c$(S → L) on the acidity function $h_0$. The directionality of the chemical wave propagation is maintained through a wide range of $h_0$. This agrees qualitatively with the experimental result shown in Figure 10.

## Conclusions

In this study, we found a unidirectional propagation of the chemical waves through a catalyst-less gap separating two fixed-catalyst BZ media with different thicknesses. We show that the

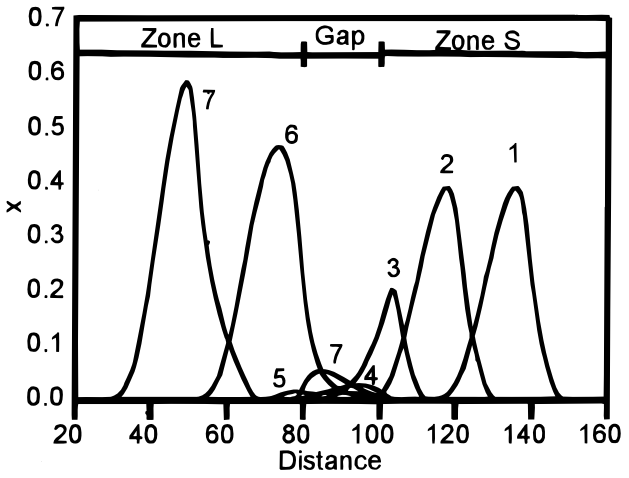


**Figure 13.** Concentration profiles of $x$ along the spatial axis (Grid points) at equal time intervals for the S → L propagation. The left and the right of the gap are the zones with thickness of 60 $\mu$m (zone L) and 30 $\mu$m (zone S), respectively ($\eta = 30$ $\mu$m, $\epsilon = 4.52 \times 10^{-1}$, $q = 0.5$, $\alpha = 4.25 \times 10^{-3}$, $\beta = 3.4 \times 10^{-3}$, $\mu = 5.1 \times 10^{-4}$, $\Delta\tau = 5 \times 10^{-3}$, $h_0 = 0.4$).

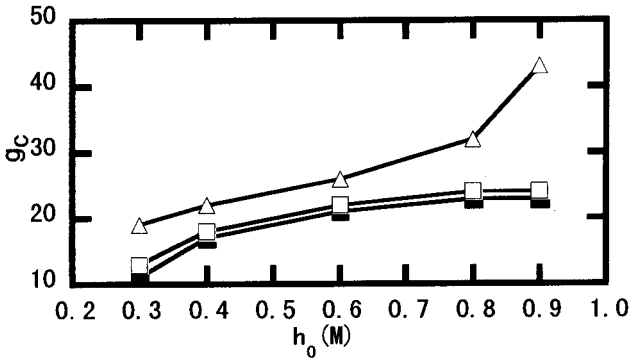


**Figure 14.** Dependence of the $g_c$(S → S) (■), $g_c$(L → S) (□), and $g_c$(S → L) (△) on $h_0$. The values of $g_c$'s are represented by the numbers of grid points in the gap, where one grid point corresponds to 5 $\mu$m. To introduce the dependence of $\eta$ on $h_0$, we assume that $\eta$ can be given by $\eta = \eta_0/h_0$, where $\eta_0$ is a constant reflecting the magnitude of the dissipation of the activator. For $h_0 < 0.25$, the zone S loses its excitability. For $h_0 > 0.97$, the zone L becomes oscillatory ($\eta_0 = 12$ $\mu$m·M, $\epsilon = 4.52 \times 10^{-1}$, $q = 0.5$, $\alpha = 4.25 \times 10^{-3}$, $\beta = 3.4 \times 10^{-3}$, $\mu = 5.1 \times 10^{-4}$, $\Delta\tau = 5 \times 10^{-3}$).

existence of the catalyst-less gap and the asymmetry of the excitability of BZ media at both sides of the gap play the most important roles in the unidirectional propagation of the chemical wave. We also show that a simple model, in which the dissipation of the activator through the membrane surface is assumed, can reproduce the qualitative aspects of the experimental results.

In addition, this experiment suggests the existence of a variety of similar excitable systems that realize the unidirectional propagation of excitation waves. In short, a pair of different excitable media coupled via diffusive interaction might realize the unidirectional propagation of excitation waves only by changing the strength of the interaction. Regarding the BZ reactions, a variety of these systems can be established using BZ media with different catalysts, different catalyst concentrations, different oxygen concentrations, different intensities of light illumination, different temperatures, and so on.

Finally, this type of unidirectional propagation provides insight into the pattern formation of excitation waves especially in biological system, because spatial inhomogeneity of excitability is common in biological excitable media.

## References and Notes

(1) Winfree, A. T. *J. Theor. Biol.* **1967**, *16*, 15.
(2) Winfree, A. T. *Science* **1972**, *175*, 634.
(3) Winfree, A. T. *Geometry of Biological Time*; Springer-Verlag: New York, 1990.
(4) Zaikin, A. N.; Zhabotinsky, A. M. *Nature* **1970**, *225*, 535.
(5) Field, R. J., Burger, M., Eds. *Oscillation and Traveling Waves in Chemical Systems*; Wiley: New York, 1984.
(6) Scott, S. K. *Oscillations, Waves, and Chaos in Chemical Kinetics*; Oxford University Press: Oxford, U.K., 1994.
(7) Maselko, J.; Showalter, K. *Nature* **1989**, *339*, 609.
(8) Maselko, J.; Reckley, J. S.; Showalter, K. *J. Phys. Chem.* **1989**, *93*, 2774.
(9) Lázár, A.; Noszticzius, Z.; Försterling, H. D.; Nagy-Ungvarai, Z. *Physica D* **1995**, *84*, 112.
(10) Steinbock, O.; Kettunen, P.; Showalter, K. *Science* **1995**, *269*, 1857.
(11) DeSimone, J. A.; Beil, D. L.; Scriven, L. E. *Nature* **1973**, *180*, 946.
(12) Linde, H.; Zirkel, C. *Z. Phys. Chem.* **1991**, *174*, 145.
(13) Swinney, H. L., Krinsky, V. I., Eds. *Waves and Patterns in Chemical and Biological Media*; MIT Press: Cambridge, MA, 1992.
(14) Agladze, K.; Keener, J. P.; Müller, S. C.; Panfilov, A. *Science* **1994**, *264*, 1746.
(15) Zhabotionsky, A. M.; Eager, M. D.; Epstein, I. R. *Phys. Rev. Lett.* **1993**, *71*, 1526.
(16) Volford, A.; Noszticzius, Z.; Krinsky, V.; Dupont, C.; Lázár, A.; Försterling, H. D. *J. Phys. Chem. A* **1998**, *102*, 8355.
(17) Zhabotinsky, A. M.; Györgyi, L.; Dolnik, M.; Epstein, I. R. *J. Phys. Chem.* **1994**, *98*, 7981.
(18) Bugrim, A. E.; Zhabotinsky, A. M.; Epstein, I. R. *J. Phys. Chem.* **1995**, *99*, 15930.
(19) Agladze, K.; Aliev, R. R.; Yamaguchi, T.; Yoshikawa, K. *J. Phys. Chem.* **1996**, *100*, 13895.
(20) Kusumi, T.; Yamaguchi, T.; Aliev, R. R.; Amemiya, T.; Ohmori, T.; Hashimoto, H.; Yoshikawa, K. *Chem. Phys. Lett.* **1997**, *355*, 271.
(21) Yoshikawa, K.; Motoike, I.; Kajiya, K. *IEICE Trans. Electron.* **1997**, *E80-C*, 931.
(22) Dopont, C.; Agladze, K.; Krinsky, V. *Physica A* **1998**, *249*, 47.
(23) Agladze, K.; Dupont, C.; Krinsky, V. *Nuovo Cimento D* **1998**, *20D*, 103.
(24) Suzuki, K.; Yoshinobu, T.; Iwasaki, H. *Jpn. J. Appl. Phys.* **1999**, *38*, L345.
(25) Aliev, R. R.; Agladze, K. I. *Physica D* **1991**, *50*, 65.
(26) Yoshikawa, K.; Aihara, R.; Agladze, K. *J. Phys. Chem. A* **1998**, *102*, 7649.
(27) Rovinsky, A. B.; Zhabotinsky, A. M. *J. Phys. Chem.* **1984**, *88*, 6082.
(28) Rovinsky, A. B. *J. Phys. Chem.* **1986**, *90*, 217.
(29) Aliev. R. R.; Rovinsky, A. B. *J. Phys. Chem.* **1992**, *96*, 732.
(30) Winston, D.; Arora, M.; Maselko, V.; Gáspár, V.; Showalter, K. *Nature* **1991**, *351*, 132.
(31) Amemiya, T.; Nakaiwa, M.; Ohmori, T.; Yamaguchi, T. *Physica D* **1995**, *84*, 103.